Evol Biol (2011) 38:144–162
DOI 10.1007/s11692-011-9110-2

RESEARCH ARTICLE

Evolutionary Lability of Integration in Cambrian Ptychoparioid Trilobites

Mark Webster · Miriam L. Zelditch

Received: 20 December 2010 / Accepted: 17 February 2011 / Published online: 1 March 2011

Abstract Phenotypic integration can influence evolutionary rate and direction by channeling variation into few dimensions. The extent to which that channeling serves as a constraint over macroevolutionary timescales is determined in part by the evolutionary lability of phenotypic integration. Evolutionary change in patterns of pleiotropy, potentially reducing that constraint, is thought to be more readily achieved when pleiotropy is structured by variation arising in parallel along different developmental pathways rather than by variation arising from direct interactions within and between those pathways. Herein we test two predictions that follow from that hypothesis: (1) that clades undergoing dramatic diversification are characterized by integration that is weakly influenced by direct interactions; and (2) that the structure of integration arising from direct interactions is more conservative than that arising from parallel variation. We examine integration of the cranidium of two Cambrian ptychoparioid trilobites, *Crassifimbra walcotti* and *Eokochaspis nodosa*, comparing them to each other and to a previously studied species, *C.*? *metalaspis*. Shape variation is decomposed into components representing variation among individuals and variation due to direct interactions. In all three species, variation among individuals was only weakly influenced by direct interactions, suggesting that integration was unlikely to have been a long-term constraint on the Cambrian diversification of ptychoparioids. Phenotypic integration of *E. nodosa* is no more similar than expected by chance to either *Crassifimbra* species, but the component due to direct interactions is more similar than expected by chance to that of *C.*? *metalaspis*. Conversely, the two *Crassifimbra* species are generally similar (although not identical) in phenotypic integration, but markedly differ in their structure of direct interactions. Integration arising from direct interactions was therefore not immune to restructuring over even short evolutionary timescales, and was not always more conservative than that arising from parallel variation.

Keywords Integration · Modularity · Cambrian · Trilobites · Evolution · Morphometrics

M. Webster (✉)
Department of the Geophysical Sciences, University of Chicago, 5734 South Ellis Avenue, Chicago, IL 60637, USA
e-mail: mwebster@geosci.uchicago.edu

M. L. Zelditch
Museum of Paleontology, University of Michigan, Ann Arbor, MI 48109-1079, USA

Introduction

Phenotypic integration refers to interdependencies among morphological traits that arise from functional and/or developmental coupling between them—couplings that are expected to promote the evolution of correlations (Olson and Miller 1958; Riedl 1978; Cheverud 1982, 1984; Schlosser and Wagner 2004). Understanding the structure of integration is important because that structure can impose a constraint on patterns of diversification that can either impede or enhance the rate of evolution depending on the topography of the adaptive landscape (Simpson 1944; Burger 1986; Wagner 1988; Wagner and Altenberg 1996; Schluter 1996; Marroig and Cheverud 2005; Renaud et al. 2006; Sniegowski and Murphy 2006; Hunt 2007). Integration may be most likely to impede rapid diversification in diverse directions, the hallmark of an adaptive radiation, by restricting change to one or a few dimensions. In this evolutionary context, modularity (approximately the converse of integration) may enable rapid diversification because modularity allows

individual parts to evolve independently without interference from others (Wagner and Altenberg 1996). As a result, the evolutionary relationships among parts can differ along phylogenetic branches, leading to changes in diverse directions. But the extent to which macroevolutionary diversification is constrained by phenotypic integration over the long term depends, in part, on the lability of the structure of integration: if this itself evolves rapidly, the directions of "least resistance" reorient, making the restriction of change along those particular directions unlikely to constrain diversification over the long term.

The lability of integration may be influenced by its developmental and functional origins. It is clear that developmental interactions must have a strong impact on phenotypic integration because developmental interactions are the proximate cause of phenotypic correlations. It is less clear that functional coupling has a strong impact on phenotypic integration even though numerous studies have shown that integration can be predicted from theories of function (e.g., Cheverud 1982; Kingsolver and Wiernasz 1987; Zelditch and Carmichael 1989; Jernigan et al. 1994; Goswami 2006a, b): the generality of that explanation has not been broadly assessed. Indeed, among arthropods, phenotypic correlations are structured by the developmental origins of body plan traits (Cowley and Atchley 1990), and a recent study has shown that functional integration is a poor predictor of phenotypic integration in cricket wings (Klingenberg et al. 2010). If phenotypic integration is due largely to development, especially to highly conserved processes, it may be unable to adapt to changes in the adaptive topography when function evolves.

That adaptability may depend on the developmental origin of the correlation. Two distinct classes of developmental causes of integration have been identified according to their origin—classes hypothesized to differ in their evolutionary flexibility. One is parallel variation, whereby the same source of variation (genetic or environmental) acts independently in two or more developmental modules. For example, variation in a gene that is expressed in two or more modules induces a correlation between traits originating within those different modules. The other is direct interactions, whereby variation is transmitted within and between developmental pathways that directly connect to each other (e.g., Klingenberg and Zaklan 2000; Klingenberg et al. 2001, 2003; Klingenberg 2004, 2005, 2008). For example, any variation in a gene expressed upstream in a developmental pathway induces integration among downstream traits. This distinction between classes of developmental causes of integration matters because integration arising from parallel variation is arguably more easily modified than that arising from direct interactions. That is because parallel variation can be modified by selection for favorable patterns of pleiotropy, whereas altering the network of direct interactions may require a fundamental restructuring of developmental pathways (Klingenberg 2004, 2005, 2008).

This hypothesis about the relative lability of the two classes of developmental causes of integration leads to two predictions: (1) clades undergoing dramatic diversification should be characterized by phenotypic integration that is only weakly influenced by direct interactions; and (2) the structure of integration arising from direct interactions should be more conservative than that arising from parallel variation. Few studies have assessed the impact of direct interactions on phenotypic integration, making it difficult to predict whether direct interactions are likely to have a strong influence in any particular case. Several studies have examined that impact on extant insect wings (Klingenberg and McIntyre 1998; Klingenberg and Zaklan 2000; Klingenberg et al. 2001; Breuker et al. 2006; Debat et al. 2006), mammalian skulls (Debat et al. 2000; Hallgrímsson et al. 2004; Drake and Klingenberg 2010) and mandibles (Klingenberg et al. 2003; Badyaev and Foresman 2004; Young and Badyaev 2006; Zelditch et al. 2008, 2009), cichlid jaws (Klingenberg et al. 2002), and an extinct trilobite cranidium (Webster and Zelditch 2011). The diversity of conclusions is difficult to interpret owing to the varied analytical methods, which also make it difficult to generalize across studies (Klingenberg 2008, p. 124; Drake and Klingenberg 2010, p. 299). Moreover, and perhaps more importantly, most studies analyze just one species so data that are capable of testing the hypothesis that integration due to direct interactions is more conserved than that due to parallel variation are sparse. That lack of data regarding the relative conservatism of integration due to direct interactions also makes it difficult to discern any causal relationship between the origin of integration and rates of diversification. One of the few studies that examined the relative conservatism of integration due to direct interactions, and that also examined their impact on diversification, involves a classic case of rapid diversification, that of domestic dogs (Drake and Klingenberg 2010). Drake and Klingenberg concluded that phenotypic integration is less influenced by direct interactions in the domestic dog than in the wolf, as would be anticipated if integration due to direct interactions limits diversification, and that, while the two species are generally similar in the structure of both phenotypic integration and direct interactions, they are considerably more similar in direct interactions, as would be anticipated if direct interactions are conserved. Similarly, macaque and mouse skulls were found to be more similar in their structure of direct interactions than in their structure of phenotypic integration (Hallgrímsson et al. 2004). In terms of mandibular integration, the structure of both phenotypic integration and that due specifically to direct interactions is generally conserved across nine species of soricid shrews (Young and Badyaev 2006), and the mandibles of two distantly related rodents (a

sciuromorph [fox squirrel] and a myomorph [prairie deer mouse]) are no more similar in the structure of integration due to direct interactions than in the overall structure of phenotypic integration (Zelditch et al. 2009).

Here we investigate the structure of phenotypic integration in the trilobite cranidium, assessing the contribution of direct interactions to integration in two early ptychoparioid trilobite species: *Crassifimbra walcotti* (Resser 1937) and *Eokochaspis nodosa* Sundberg and McCollum 2000 (Fig. 1a–d). We compare their correlation structures, both their overall pattern of phenotypic integration (due to variation among individuals) and that due to direct interactions. We compare both species to another Cambrian ptychoparioid trilobite, *Crassifimbra*? *metalaspis* (Sundberg and McCollum 2000) (Fig. 1e, f), the subject of our early study (Webster and Zelditch 2011). In that study, we found that phenotypic integration was only weakly influenced by direct interactions; this was anticipated in that early ptychoparioids are thought to be the ancestral stock from which more derived trilobite clades arose during the Cambrian (Fortey in Whittington et al. 1997, p. 296; Fortey 2001, p. 1148). *Crassifimbra walcotti* is very closely related to and stratigraphically coeval with *C.*? *metalaspis*, whereas *E. nodosa* shares less recent common ancestry with the two *Crassifimbra* species and occurs in slightly younger strata (Webster 2011; "Appendix"). We again focus on the cranidium (Figs. 1, 2), a morphologically complex cephalic sclerite well suited for analysis of shape using landmarks and semilandmarks. A variety of structures are incorporated into the cranidium, associated with different functions (Whittington et al. 1997; below). A modular arrangement of parts within such a multi-function sclerite might therefore be expected. Diversification of cranidial shape was a major component of trilobite evolution (Foote 1989, 1990, 1991, 1993a, b; Fortey and Owens in Whittington et al. 1997).

The paper is structured as follows. We first test the hypothesis that functional integration predicts the structure of correlations. We restrict that analysis to function because the functional attributes of trilobite cranidial regions are relatively well understood but their developmental and genetic regulators are not. Given that we have only one hypothesis for cranidial integration (one that we show to fit poorly), we also examine the structure of integration in *C. walcotti* and *E. nodosa* using exploratory methods. We then statistically assess the contribution of direct interactions to phenotypic integration in both species and compare the structure of overall phenotypic integration to that arising from direct interactions. Finally, we compare *C. walcotti*, *C.*? *metalaspis*, and *E. nodosa* to determine whether direct interactions are historically conserved, as expected.

Functional Integration of the Cranidium

The function of the various structures incorporated into the cranidium is relatively well established (Whittington et al. 1997): the glabella covered the stomach and anterior

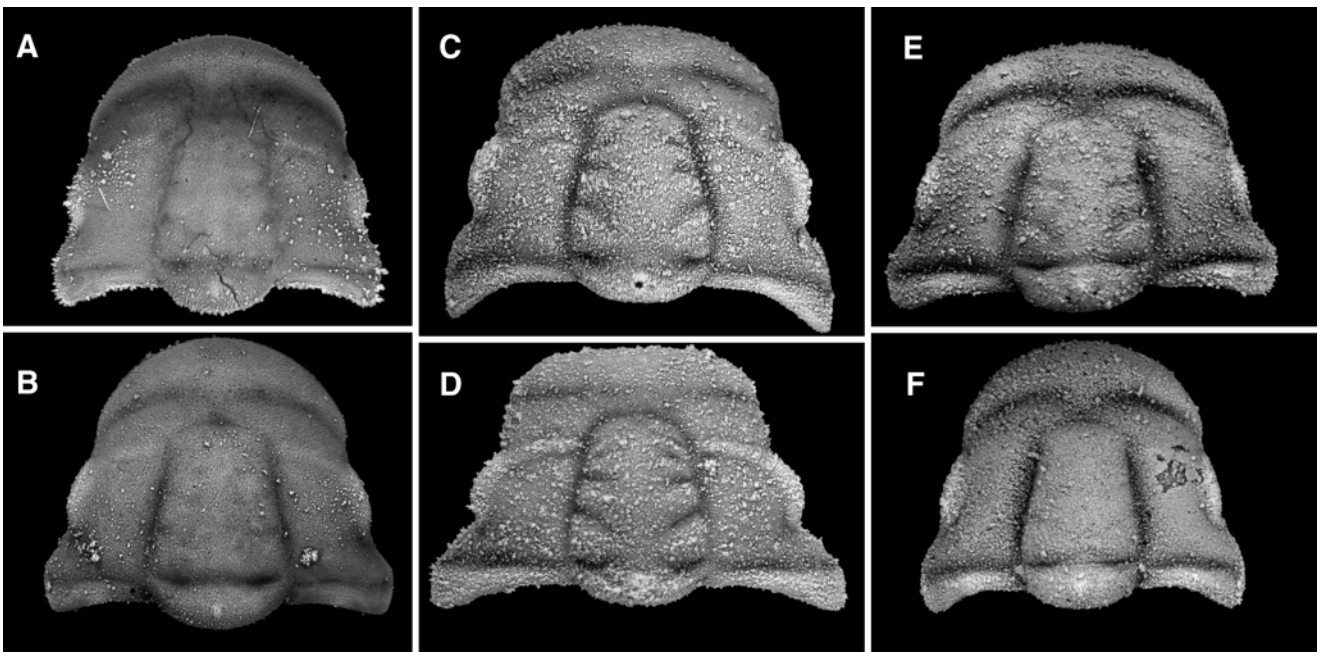

Fig. 1 Representative silicified cranidia of *Crassifimbra walcotti* (**a**,**b** from collection ICS-1029), *Eokochaspis nodosa* (**c**,**d** from collection ICS-1192), and *C.*? *metalaspis* (**e**,**f** from collection ICS-10124) in dorsal view. **a** FMNH PE58242, ×12. **b** FMNH PE58247, ×11. **c** FMNH PE58291, ×9. **d** FMNH PE58294, ×9. **e** FMNH PE58271, ×9. **f** FMNH PE58273, ×9

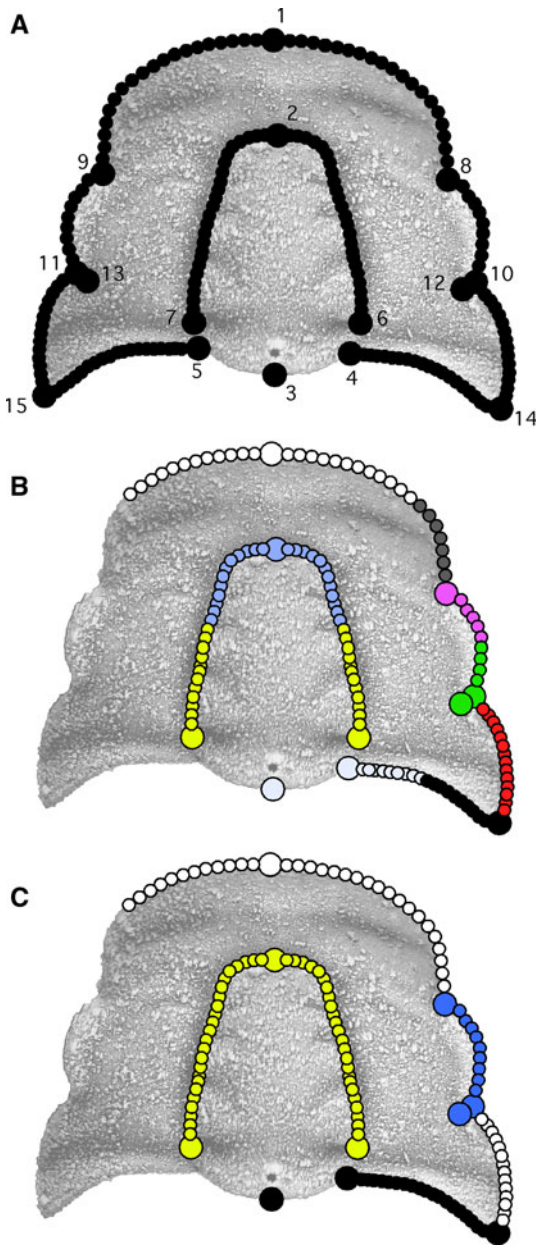

Fig. 2 **a** Landmark and semilandmark selection on the cranidium of *Eokochaspis nodosa*. Landmarks (*large circles*, *numbered*): *1*, Anterior cranidial margin on sagittal axis; *2*, anterior of glabella on sagittal axis; *3*, posterior margin of occipital ring on sagittal axis; *4*,*5*, intersection of occipital ring and posterior cranidial margin in dorsal view; *6*,*7*, intersection of SO with axial furrow; *8*,*9*, anterior tip of palpebral lobe; *10*,*11*, posterior tip of palpebral lobe; *12*,*13*, intersection of posterior facial suture with distal margin of palpebral lobe in dorsal view; *14*,*15*; distal tip of posterior wing of fixigena. Semilandmarks (*small circles*, *not numbered*) summarize curvature of anterior cranidial margin and anterior branch of the facial suture (19 points each side between landmarks 1 and 8/9), distal margin of palpebral lobe (9 points each side between landmarks 8/9 and 10/11), posterior branch of the facial suture (14 points each side between landmarks 10/11 and 14/15), posterior cranidial margin (19 points each side between landmarks 4/5 and 14/15), and glabella anterior to SO (24 points each side between landmarks 2 and 6/7). **b** The nine partitions of cranidial morphology analyzed herein: anterior glabella (*blue*); posterior glabella (*yellow*); anterior portion of the palpebral lobe (*purple*); posterior portion of the palpebral lobe (*green*); proximal posterior margin (*pale blue*); distal posterior margin (*black*); anterior margin (*white*); anterior branch of the facial suture (*gray*); and posterior branch of the facial suture (*red*). **c** Predicted modules in the cranidium based on the a priori functional hypothesis. Modules are associated with digestion/appendage attachment (glabella; *yellow*), the visual field (palpebral lobes; *blue*), ecdysis (facial sutures and anterior margin; *white*), and articulation between the cephalon and trunk (posterior margin; *black*)

portion of the digestive tract, and was also the site of attachment for cephalic appendages; the palpebral lobes were associated with the eye; the facial sutures were associated with ecdysis; and the posterior cranidial margin was associated with articulation between the cranidium and anterior most thoracic segment. Following Webster and Zelditch (2011), we develop a simple model for the predicted functional integration of the cranidium. The glabella, the palpebral lobes, the facial sutures, and the posterior cranidial margin are expected to represent distinct modules, based on their differing functions (associated with digestion/appendage attachment, the visual field, ecdysial mechanics, and cephalon-trunk articulation mechanics, respectively). The anterior cranidial margin is assigned to the ecdysial functional module given its close association with the rostral suture, which lies subparallel and immediately interior to the anterior margin on the ventral surface.

To assess the fit of the functional model to the data, we divide the cranidium into nine partitions and represent the expected correlations among those partitions (Fig. 2c) by edges between nodes of a graph. In specifying the model, correlations between edges within a module are free parameters, estimated by maximum-likelihood, whereas edges between modules are fixed because modules are expected to be conditionally independent. The fit of the model to the data is then assessed by the deviance between them, which is a function of deviation between the model and data and sample size. The null hypothesis is that the model does fit the data, thus a low P value (<0.05) indicates that the deviance between the model and data is significantly greater than expected by chance. Because models with few fixed parameters are likely to fit well, judged solely by their χ^2-values relative to their degrees of freedom, we also use the Akaike Information Criterion (AIC) to determine whether the hypothesis of functional integration improves upon the null model of complete integration (i.e., the saturated model). The AIC is $2k - 2\ln(L)$, where k is the number of parameters and L is the maximized value of the likelihood function (Akaike 1974); the model with the lower AIC is therefore preferred. We also assess the fit of the functional model by another

approach: the correlation between the expected and observed among-partition correlation matrices. To construct the expected correlation matrix, we assign a correlation of 1.0 to partitions hypothesized to belong to the same functional module, and a correlation of zero to partitions hypothesized to belong to different modules. The fit of this model is tested for its statistical significance using the permutation-based Mantel test, which randomly permutes rows and columns in one matrix and computes the correlation between matrices, producing a distribution of correlation coefficients under the null hypothesis that the two matrices are randomly related (Mantel 1967; Dietz 1983).

Materials and Methods

Material

Silicified sclerites of *C. walcotti* (Fig. 1a, b) and *E. nodosa* (Fig. 1c, d) were recovered from the Pioche Formation, east-central Nevada (Webster 2011). For each species, the material analyzed herein was extracted from a single, well-constrained horizon at a single locality: *C. walcotti* from collection ICS-1029 (sampled from carbonate nodules 11 meters below the top of the Combined Metals Member, uppermost Dyeran [traditional "Lower Cambrian" of Laurentia], Oak Spring Summit section); and *E. nodosa* from collection ICS-1192 (sampled from the ribbon carbonate marking the base of the Comet Shale Member, lowermost Delamaran [traditional "Middle Cambrian" of Laurentia], Ruin Wash section). The bed in the Oak Spring Summit section from which collection ICS-1029 was made is approximately coeval with the bed at the Log Cabin Mine section from which the previously studied silicified material of *C.*? *metalaspis* was recovered (collection ICS-10124; Webster 2011; Webster and Zelditch 2011). (Phylogenetic relationships among these three species and tentative divergence times are discussed in the "Appendix".) Taphonomic and stratigraphic data indicate that these three beds represent comparable, minimally time-averaged accumulations (Webster 2011). The carbonates were dissolved in weak acetic acid and silicified sclerites were picked from the insoluble residue. Cranidia were cleaned, blackened with dilute Indian ink, whitened with ammonium chloride, and mounted for photography using the standard orientation of Shaw (1957), with the dorsal surface of the palpebral lobes being positioned horizontally below a vertically mounted digital camera. Each cranidium was whitened, mounted, and photographed twice; approximately 2 weeks separated repeated imaging of each specimen.

Cranidia of *C. walcotti* included in the analyses presented herein range from 0.99 to 4.37 mm in sagittal length ($n = 35$); those for *E. nodosa* range from 1.68 to 4.21 mm in sagittal length ($n = 35$). These size ranges are comparable to those from the previously studied sample of *C.*? *metalaspis* (1.71–5.43 mm in sagittal length, $n = 72$; Webster and Zelditch 2011). Specimens are housed in the Field Museum of Natural History, Chicago (FMNH) and the Institute for Cambrian Studies, University of Chicago (ICS).

Quantifying Cranidial Shape

Landmark-based geometric morphometrics methods were used to analyze the structure of integration within the cranidium of each species. The *x*- and *y*-coordinates of 15 landmarks and 170 semilandmarks (along 10 curves) were digitized on cranidia of each species (Fig. 2a). These represent the same sampling of cranidial shape used in the previous study of *C.*? *metalaspis* (Webster and Zelditch 2011). Coordinate data were restricted to two dimensions because the cranidia are small in absolute size (making error associated with digitizing in the *z*-plane relatively large) and are of relatively low relief. It is assumed that exclusion of the third dimension does not markedly affect the conclusions. Landmark and outline coordinates were digitized using tpsDig2 (Rohlf 2009). Coordinates of sliding semilandmarks were calculated from the curve data by minimizing the Procrustes distance between each individual's curve and the reference curve; sliding was done by SemiLand6 (Sheets 2009).

Ontogenetic allometry can be a cause of covariances, but one that is due to the age-heterogeneity of the sample rather than to variation among individuals at any one developmental stage. Allometry is a weak but significant contributor to cranidial shape variation in both *C. walcotti* and *E. nodosa*, as assessed by the regression of shape on size (estimated by the natural logarithm of centroid size [ln CS]). In both species, the null hypothesis of isometric growth is rejected (for *C. walcotti*, 48% of variance explained by the regression, $P < 0.001$; for *E. nodosa*, only 7% of variance explained by the regression, but $P = 0.041$). The shape variation associated with size was removed by adding the residuals from the regression to the shape expected at ln CS of 3.7, equivalent to a sagittal cranidial length of approximately 4.3 mm for *C. walcotti* and of approximately 3.8 mm for *E. nodosa*. This is close to the maximum size (but within the size range) of sampled specimens for each species, and therefore does not involve extrapolating beyond the observed portion of ontogeny. This size-standardization was performed using Standard6 (Sheets 2001).

Isolating Integration Resulting from Direct Interactions Among Developmental Pathways

We use correlations of (signed) deviations from bilateral asymmetry (i.e., correlations of fluctuating asymmetry, FA) to infer regions that are integrated through direct interactions (Klingenberg and Zaklan 2000; Klingenberg et al. 2001, 2003; Klingenberg 2005; Zelditch et al. 2008, 2009; Webster and Zelditch 2011). FA provides information about direct interactions by holding the causes of parallel variation constant, i.e., the genetic and environmental factors that generate the (co)variances in two or more otherwise independent modules (e.g., Klingenberg and Zaklan 2000; Klingenberg et al. 2001, 2003; Klingenberg 2005). Because both genotype and environment are constant across sides, these two potential causes of integration cannot explain correlated random deviations from symmetry. Instead, these correlations are caused by the mechanisms that transmit variation within and between developmental pathways.

The FA component of variation is tested for its statistical significance using the standard two-factor mixed-model analysis of variance (ANOVA), with the two main effects being "Individuals" and "Sides" (Leamy 1984; Palmer and Strobeck 1986). The Individuals component quantifies the variation among individuals after correction for asymmetry; the Sides effect quantifies the directional asymmetry between left and right sides of the organism; and FA is quantified by the interaction between these two components. The statistical significance of FA is assessed by the F ratio between the interaction mean square and measurement error mean square (Leamy 1984; Palmer and Strobeck 1986). That approach has been adapted to Procrustes-based methods of shape analysis (Auffray et al. 1996; Klingenberg and McIntyre 1998; Klingenberg et al. 2002). A permutation test is used to determine the significance of the FA term. The analysis of FA was conducted in SAGE (Márquez 2007a), which generates shape coordinates for the Individuals and FA components used in subsequent analyses.

Estimating Correlation Matrices

To estimate the correlations between the shape of cranidial regions we divided it into nine partitions (Fig. 2b): (1) anterior glabella; (2) posterior glabella; (3) anterior portion of the palpebral lobe; (4) posterior portion of the palpebral lobe; (5) proximal portion of the posterior cranidial margin (including a landmark at the midline of the posterior margin of the occipital ring); (6) distal portion of the posterior cranidial margin; (7) anterior cranidial margin; (8) anterior branch of the facial suture; and (9) posterior branch of the facial suture. The boundary between partitions (1) and (2) corresponds to the transition from the region of the glabella that proportionally narrows during ontogeny versus the region that proportionally widens during ontogeny (Webster 2011). The boundary between partitions (3) and (4) corresponds to a break in curvature on the distal margin of the palpebral lobe seen on some specimens, but is otherwise arbitrary. The boundary between partitions (5) and (6) corresponds to the location of the fulcrum (distal to which the cranidial margin is oriented more strongly posterolaterally and ventrally). The boundary between partitions (7) and (8) approximately corresponds to the contact between the anterior cranidial margin and the anterior branch of the facial suture, although this transition is often not marked by a distinct break in curvature.

Following Monteiro et al. (2005), we examined correlations between shapes of partitions to estimate integration. Partitions (1), (2), and (7) are bilaterally symmetric so their shapes are described by landmarks on both sides of the sagittal axis (Fig. 2b). The other partitions display matching symmetry and are described by landmarks on one side of the cranidium (Fig. 2b). Each partition was subsequently treated as a separate multidimensional trait, and landmark configurations for each partition were superimposed separately. The pairwise Procrustes distances between all individuals were then calculated for each partition and the matrix correlation between distance matrices of partitions was calculated, yielding a matrix of correlations between shapes of the partitions. The correlation matrix was calculated for both the Individuals and FA components of shape, permitting inference of the structure of variation among individuals (which is due to both parallel variation and direct interactions) and the integration due to direct interactions. Distance matrices and correlations between them were computed in CORIANDIS (Márquez 2007b). The resultant correlation matrix was then assessed for its fit to the a priori model (above) and subjected to a series of exploratory analyses.

Exploratory Analyses

Reticulate Network Analysis

Preliminary analysis by hierarchical clustering methods produced a poor fit between the resultant dendrograms and the data (cophenetic correlations <0.85). We therefore use an alternative method that is additive rather than ultrametric, relaxing the constraints on trait distances within and among clusters (Sattath and Tversky 1977), and that allows traits to belong to more than cluster (Makarenkov and Legendre 2004; Makarenkov et al. 2004; Zelditch et al. 2008, 2009; Webster and Zelditch 2011). Reticulations are added if they significantly improve the additive dendrogram, based on an optimization between fit to the

original distances and the number of linkages on the dendogram. Reticulate network analysis was conducted on the among-partition correlation matrices using T-REX (Makarenkov 2000), employing the conservative Q_1 optimization criterion for addition of reticulations (as summarized by Zelditch et al. 2008, 2009).

Graphical Modeling

Graphical modeling is another useful method for exploring the structure of integration (Magwene 2001; Young 2004; Young and Hallgrímsson 2005; Polanski and Franciscus 2006; Allen 2008; Lawler 2008; Zelditch et al. 2009; Webster and Zelditch 2011; but see criticisms by Mitteroecker and Bookstein 2007, 2009; reply by Magwene 2009). The analysis is done by analyzing correlations among pairs of variables, conditional on all others. When used in an exploratory fashion, a heuristic search can be done to find a model that best reconstructs the observed associations among variables with as few edges as possible. Heuristic searches were done in a stepwise fashion, using the options for a headlong search (i.e., edges inspected in random order), a bidirectional search (i.e., both adding and deleting edges), and an unrestricted search (i.e., allowing edges that were removed in a prior iteration to be reconsidered); for more details see the summary by Zelditch et al. (2009). An F test was used to determine the significance of the edges given our relatively small sample size. The edge strength between partitions (E_{ij}) provides a measure of the information that the traits provide about each other, conditional on all other traits, and is calculated as $E_{ij} = -0.5 \times \ln(1 - (p^2_{ij.k}))$ where $p_{ij.k}$ is the partial correlation between partitions i and j. An edge strength >0.025 is deemed strong (Lawler 2008, p. 208). Graphical modeling was done in MIM 3.2.0.7 (Edwards 2008).

Assessing the Contribution of Direct Interactions to Phenotypic Integration

To test the hypothesis that integration due to direct interactions is weak in clades undergoing dramatic diversification (such as early ptychoparioids), we estimated the contribution of direct interactions to phenotypic integration in each species. This was done by comparing the correlation matrices based on the variation among individuals and the (signed) FAs (e.g., Klingenberg and Zaklan 2000; Klingenberg et al. 2003; Klingenberg 2005; Zelditch et al. 2008, 2009; Webster and Zelditch 2011). The comparison was made by estimating the matrix correlation between the two correlation matrices. The statistical significance of this correlation was then assessed by two approaches that differ in their null hypotheses. The first uses a conventional Mantel test, with the null hypothesis being that the two matrices are no more similar than expected by chance. A statistically significant correlation means that the structure of phenotypic integration is more similar to that of direct interactions than expected by chance, implying that direct interactions make a significant contribution to phenotypic integration. The alternative approach tests the null hypothesis that the two matrices are no more different than expected by chance; i.e., that the samples are drawn from a single population with a single correlation structure and therefore that any deviation from a matrix correlation of 1.0 is due to chance. Testing this null hypothesis has previously been done using common principal components analysis (Cheverud and Marroig 2007; Hunt 2007) or random skewers (Cheverud and Marroig 2007), or by comparison of an observed matrix correlation to either (1) the repeatability of a matrix with itself (Hallgrímsson et al. 2006), or (2) the distribution of dissimilarities between simulated random samples drawn from a pooled similarity matrix (Hunt 2007). Given our small sample sizes, and our use of correlation rather than covariance matrices, we test this null hypothesis using a novel bootstrapping procedure broadly analogous to the methods employed by Hallgrímsson et al. (2006) and Hunt (2007). According to this procedure, a correlation matrix with dimensions $n \times p$ (where n = sample size for that correlation matrix and p = number of traits) is generated by drawing numbers randomly from a multivariate normal distribution and then imposing the structure of the observed correlation on the random matrix. This procedure is repeated 1,000 times, and the matrix correlations are estimated between the simulated matrices, generating a distribution of matrix correlations between matrices that differ only by random, normally distributed noise. The matrix correlation between the hypothesized and target matrix, or between two observed correlation matrices, can then be compared to the distribution obtained from the simulated matrices. The probability of obtaining a matrix correlation as low as the one between observed samples when the matrices differ by no more than expected by chance is given by the proportion of bootstrapped distributions that have a lower matrix correlation (Haber, unpublished; R code available at http://www.geosci-people.uchicago.edu/profiles/mwebster).

Comparing the Structure of Integration Among Species

In order to test the second hypothesis—that the structure of integration arising from direct interactions is phylogenetically more conservative than that arising from parallel variation—we compared the correlation structure of the Individuals component, and that of the (signed) FA component, between species. Similarity of the correlation matrices was quantified using matrix correlation. The significance of the matrix correlation was tested using the two approaches outlined above.

Results

Isolating Integration Resulting from Direct Interactions Among Developmental Pathways

Variation among individuals (the Individuals component in Tables 1, 2) accounts for the vast majority of variation in both *C. walcotti* and *E. nodosa*. As expected for the bilaterally symmetrical cranidium, very little of the variation is explained by the difference between the left and right sides. FA accounts for approximately 10% of the total shape variation in both species, and it is statistically highly significant. Measurement error in the *C. walcotti* sample accounts for almost as much of the total shape variance (8%) as does the FA term (Table 1), perhaps due to the smaller average size of cranidia (1.88 mm sagittal length) in this sample relative to that of *E. nodosa* (2.65 mm) and the associated greater difficulty in consistent mounting of specimens for photography. Nevertheless, the mean square of the FA term is almost three times that of the measurement error term, and the FA term in the *C. walcotti* sample is therefore deemed biologically interpretable (albeit cautiously).

Correlation Matrices

Crassifimbra walcotti

The correlation matrix for the Individuals component of variation is shown in Table 3 (lower triangle). The anterior glabella is significantly correlated with the proximal posterior margin and the anterior branch of the facial suture. The proximal posterior margin is also significantly correlated with the posterior glabella and the anterior margin partitions. The anterior and posterior portions of the palpebral lobe are not significantly correlated with each other; indeed, the former is not significantly correlated with any other partition although it does show a relatively strong correlation with the anterior branch of the facial suture. The posterior palpebral lobe partition is significantly correlated with the distal posterior margin and anterior branch of the facial suture. The posterior palpebral lobe also shows a high but non-significant correlation with the posterior branch of the facial suture. The posterior branch of the facial suture is significantly correlated only with the neighboring distal posterior margin, although its correlation with the anterior glabella is strong if not statistically significant. The strongest correlations are between the distal posterior margin and the posterior branch of the facial suture, and between the proximal posterior margin and the posterior glabella. None of the significant pairwise correlations between partitions were predicted by the functional hypothesis (Fig. 2c).

The correlation matrix for the FA component of variation in this species is shown in Table 3 (upper triangle). Relatively few partitions are significantly correlated: the anterior glabella partition is significantly correlated with the posterior glabella and the distal posterior margin partitions; the anterior margin significantly correlates with the proximal posterior margin; and the posterior palpebral lobe significantly correlates with the anterior branch of the facial suture. Only the last two of these associations were

Table 1 Results of the modified two-way ANOVA of size-standardized shape data for *Crassifimbra walcotti*

Effect	SS	*df*	MS	*F* value	*P* value	% Variance explained
Individuals	0.05587	6,222	0.0000090	7.9025	<0.001	78.306
Sides	0.00291	183	0.0000159	13.9973	<0.001	4.079
Individuals × sides	0.00707	6,222	0.0000011	2.6475	<0.001	9.909
Measurement error	0.00550	12,810	0.0000004	–	–	7.706
Total	0.07135					100.000

SS Sum of squares, *df* degrees of freedom, *MS* mean square

Table 2 Results of the modified two-way ANOVA of size-standardized shape data for *Eokochaspis nodosa*

Effect	SS	*df*	MS	*F* value	*P* value	% Variance explained
Individuals	0.07833	6,222	0.0000126	7.487	<0.001	83.376
Sides	0.00091	183	0.0000049	2.942	<0.001	0.964
Individuals × sides	0.01046	6,222	0.0000017	5.0667	<0.001	11.136
Measurement error	0.00425	12,810	0.0000003	–	–	4.525
Total	0.09395					100.000

SS Sum of squares, *df* degrees of freedom, *MS* mean square

Table 3 Correlation matrix for among-individual variation (derived from shape data of Individuals component of variation; lower triangle) and for direct interactions among developmental pathways (derived from shape data of FA component of variation; upper triangle) for *Crassifimbra walcotti*

	Ant Glab	Post Glab	Ant Palp	Post Palp	Prox PM	Dist PM	Ant Marg	Ant Fac	Post Fac
Ant Glab		*0.474*	0.196	0.203	0.316	*0.324*	0.189	0.296	0.093
Post Glab	0.134		0.239	0.071	0.265	0.250	0.230	0.229	0.012
Ant Palp	0.197	0.213		0.097	0.077	0.164	0.139	0.293	0.123
Post Palp	−0.007	0.047	0.034		0.106	0.165	0.094	*0.411*	0.071
Prox PM	*0.299*	*0.329*	0.040	−0.011		0.251	*0.406*	0.129	0.052
Dist PM	0.165	0.168	0.050	*0.253*	0.173		0.137	0.284	0.235
Ant Marg	0.094	0.108	0.065	0.024	*0.288*	0.115		0.274	0.003
Ant Fac	*0.293*	0.168	0.261	*−0.076*	0.324	0.037	0.150		−0.006
Post Fac	0.268	0.122	0.196	0.224	0.121	*0.375*	0.064	0.156	

Correlations significant at 95% confidence (based on 1,000 permutations) are italics

Partition abbreviations: *Ant Glab* anterior glabella, *Post Glab* posterior glabella, *Ant Palp* anterior portion of palpebral lobe, *Post Palp* posterior portion of palpebral lobe, *Prox PM* proximal portion of posterior margin, *Dist PM* distal portion of posterior margin, *Ant Marg* anterior margin, *Ant Fac* anterior branch of facial suture, *Post Fac* posterior branch of facial suture. For partition locations see Fig. 2b

Table 4 Correlation matrix for among-individual variation (derived from shape data of Individuals component of variation; lower triangle) and for direct interactions among developmental pathways (derived from shape data of FA component of variation; upper triangle) for *Eokochaspis nodosa*

	Ant Glab	Post Glab	Ant Palp	Post Palp	Prox PM	Dist PM	Ant Marg	Ant Fac	Post Fac
Ant Glab		*0.429*	0.108	0.163	0.144	*0.652*	*0.406*	0.158	0.348
Post Glab	*0.353*		0.104	*0.357*	*0.342*	*0.467*	*0.523*	0.209	0.193
Ant Palp	0.098	0.199		0.224	0.167	0.012	*0.414*	0.028	0.065
Post Palp	*0.287*	0.229	−0.009		0.238	*0.357*	*0.424*	0.195	0.214
Prox PM	*0.247*	*0.409*	0.195	*0.278*		0.200	*0.327*	0.051	0.058
Dist PM	0.230	0.197	0.031	0.077	0.049		*0.416*	*0.345*	*0.586*
Ant Marg	0.043	0.136	0.082	0.179	0.111	0.122		0.134	0.251
Ant Fac	0.118	0.230	0.106	0.134	0.111	*0.422*	0.116		*0.597*
Post Fac	*0.365*	0.190	0.057	0.155	0.259	*0.440*	0.189	*0.321*	

Correlations significant at 95% confidence (based on 1,000 permutations) are italics. Partition abbreviations as for Table 3. For partition locations see Fig. 2b

also significant in the Individuals component (above). Only the significant association between the anterior and posterior glabella partitions was predicted by the functional hypothesis (Fig. 2c).

Eokochaspis nodosa

The correlation matrix for the Individuals component of variation is shown in Table 4 (lower triangle). The anterior glabella partition is significantly correlated with the posterior glabella, the posterior portion of the palpebral lobe, the posterior branch of the facial suture, and the proximal posterior margin partitions. The proximal posterior margin is also significantly correlated with the posterior glabella and posterior palpebral lobe partitions. The distal posterior margin is significantly correlated with the both facial suture partitions, which are also significantly correlated with each other. Neither the anterior margin nor the anterior portion of the palpebral lobe partitions is significantly correlated with any other partitions. The strongest correlations are found between the distal posterior margin and both branches of the facial suture, and between the proximal posterior margin and the posterior glabella. Of the significant pairwise correlations between partitions, only those between the anterior and posterior glabella partitions and between the anterior branch of the facial suture and posterior branch of the facial suture were predicted by the functional hypothesis (Fig. 2c). Only the significant correlations between the anterior glabella and proximal posterior margin partitions, the posterior glabella and proximal

posterior margin partitions, and the distal posterior margin and posterior branch of the facial suture partitions are also significant in the Individuals component of *C. walcotti*.

In stark contrast, the analysis of the FA component of *E. nodosa* reveals significant correlations between the anterior margin and all others except for the two branches of the facial suture (Table 4, upper triangle). The anterior glabella is also significantly correlated with the posterior glabella and distal posterior margin partitions, and the posterior glabella is significantly correlated with the posterior palpebral lobe plus both posterior margin partitions. The posterior palpebral lobe is also correlated with the distal posterior margin, which is also significantly correlated with both branches of the facial suture, which are significantly correlated with each other. Of these significant pairwise correlations, five were also significant in the Individuals component (i.e., those between the anterior and posterior glabella, the posterior glabella and proximal posterior margin, the distal posterior margin and anterior branch of the facial suture, the distal posterior margin and posterior branch of the facial suture, and the anterior branch of the facial suture and posterior branch of the facial suture). The strongest correlations are found between the anterior glabella and distal posterior margin, between the two branches of the facial suture, and between the posterior branch of the facial suture and the distal posterior margin. Of the significant pairwise correlations between partitions, only those between the anterior and posterior glabella, and between the anterior branch of the facial suture and the posterior branch of the facial suture were predicted by the functional hypothesis (Fig. 2c). Only the significant correlations between the anterior and posterior glabella, between the anterior glabella and distal posterior margin, and between the anterior margin and proximal posterior margin are also significant in the FA component of *C. walcotti*.

Fitting a Functional Model to Observed Correlations

The functional hypothesis fits the Individuals component of phenotypic integration moderately well in analyses based on maximum-likelihood in that the data do not deviate significantly from expectations of the functional model (Table 5). The ΔAIC values for both species are negative, indicating a better fit of the functional model than a fully saturated model to the data. However, the matrix correlation between expected and observed correlation matrices is not statistically significant, indicating that the two matrices are no more similar than expected by chance (for *C. walcotti*, $R_M = -0.136$, $P = 0.79$; for *E. nodosa*, $R_M = -0.070$, $P = 0.64$). The functional hypothesis also fits the FA component of phenotypic variation very poorly; the data deviate significantly from expectations of the model for *E. nodosa* (although not for *C. walcotti*; Table 5) and the matrix correlation between the expected and observed correlation matrices is no greater than expected by chance (for *C. walcotti*, $R_M = -0.036$, $P = 0.55$; for *E. nodosa*, $R_M = 0.082$, $P = 0.27$). The ΔAIC values reveal that the functional model shows a worse fit to the data than does the fully saturated model for *E. nodosa*. The poor fit of the functional model to the data as quantified by matrix correlation is not surprising, given that none or very few of the significant pairwise correlations between partitions were predicted by the functional hypothesis (above). The functional model also shows exceptionally poor fit to the data for both components of variation in *C.? metalaspis* (Webster and Zelditch 2011; summarized in Table 5).

Table 5 Goodness-of-fit between the observed data and the a priori hypothesis of functional integration for both the Individuals and FA components of variation, as found through graphical modeling

Observed	Component	Deviance	*df*	χ^2 *P* value	ΔAIC
C. walcotti	Individuals	31.685	30	0.382	−28.315
E. nodosa	Individuals	36.127	30	0.204	−23.873
C.? metalaspis	Individuals	98.107	30	<0.001	38.107
C. walcotti	FA	32.802	30	0.331	−27.198
E. nodosa	FA	72.673	30	<0.001	12.673
C.? metalaspis	FA	128.947	30	<0.001	68.569

χ^2 *P* values indicate the significance of the deviance between the observed data and the model. *df*, degrees of freedom. ΔAIC values indicate the difference in AIC relative to the fully saturated model

Exploratory Analyses

The reticulogram for the Individuals component of *Crassifimbra walcotti* reveals three clusters, all comprising three partitions, as well as one reticulation between two partitions that belong to different clusters (Fig. 3a). The clusters comprise the (1) posterior palpebral lobe plus distal posterior margin, both associated with the posterior branch of the facial suture; (2) anterior glabella plus anterior branch of the facial suture, both associated with the anterior palpebral lobe; and (3) anterior margin plus proximal posterior margin, both associated with the posterior glabella. The reticulation is between the anterior branch of the facial suture and the proximal posterior margin. The reticulogram for the FA component of this species also reveals three clusters and one reticulation between two partitions that belong to different clusters (Fig. 3b), but the relationships among partitions differ markedly from those revealed by analysis of the Individuals component. The clusters for the FA component comprise the (1) anterior glabella plus posterior glabella, both associated with the anterior margin plus proximal posterior margin; (2) anterior branch of the facial suture plus posterior palpebral lobe, both weakly associated with the anterior palpebral lobe; and (3)

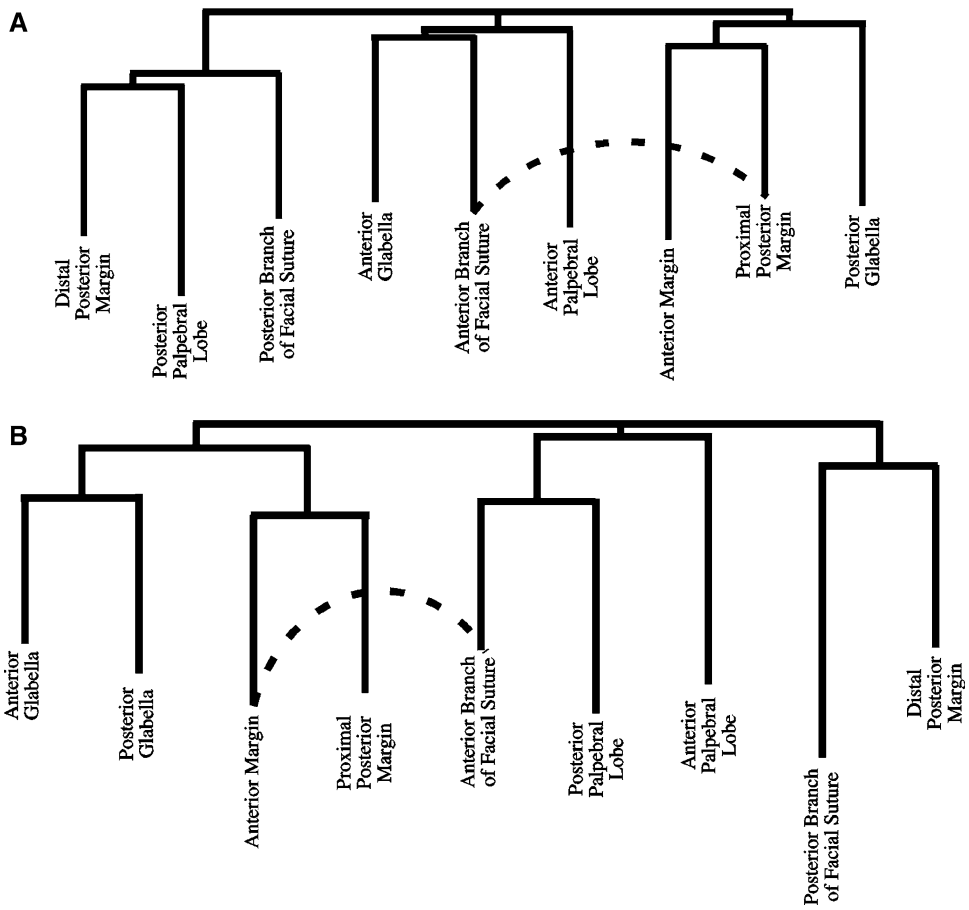

Fig. 3 Reticulograms depicting relationships among partitions for the **a** Individuals and **b** FA components of variation in *Crassifimbra walcotti*. Partitions shown in Fig. 2b

posterior branch of the facial suture plus distal posterior margin. The reticulation is between the anterior margin and the anterior branch of the facial suture partitions.

The reticulogram for the Individuals component of *E. nodosa* reveals three clusters plus one partition that is not associated with any others, and no reticulations (Fig. 4a). The clusters comprise the (1) anterior branch of the facial suture plus distal posterior margin, both associated with the posterior branch of the facial suture, and all three associated with the anterior glabella; (2) posterior glabella plus proximal posterior margin; and (3) the anterior margin plus posterior palpebral lobe. The anterior palpebral lobe is not associated with any other partition. The reticulogram for the FA component of *E. nodosa* reveals two clusters plus two partitions that are not associated with any others (Fig. 4b). The relationships among partitions do not match those revealed by analysis of the Individuals component. The clusters for the FA component comprise the (1) two branches of the facial suture, which are tightly clustered and both are associated with the anterior glabella plus distal posterior margin; those four regions are all weakly associated with the posterior glabella; and (2) anterior margin and anterior palpebral lobe. Within the first cluster, there is one reticulation: between the posterior branch of the facial suture and the distal posterior margin partitions. Neither the posterior palpebral lobe nor the proximal posterior margin is associated with any other partition.

Graphical modeling reveals a structure in the Individuals component of *C. walcotti* that is congruent with several elements of the corresponding reticulogram (Fig. 5a). There is an edge connecting the posterior branch of the facial suture to the distal posterior margin, and edges connect the proximal posterior margin to both the posterior glabella and anterior branch of the facial suture, although these last two partitions are not connected to each other. The graphical model for the FA component of *C. walcotti* (Fig. 5b) also shows some congruence with the corresponding reticulogram. Edges connect the anterior glabella and posterior glabella partitions, the anterior margin and proximal posterior margin partitions, and the posterior palpebral lobe to the anterior branch of the facial suture partitions. There is also an edge between the anterior glabella and distal posterior margin partitions, but it is weak.

The graphical model for the Individuals component of *E. nodosa* (Fig. 5c) again reveals a pattern largely

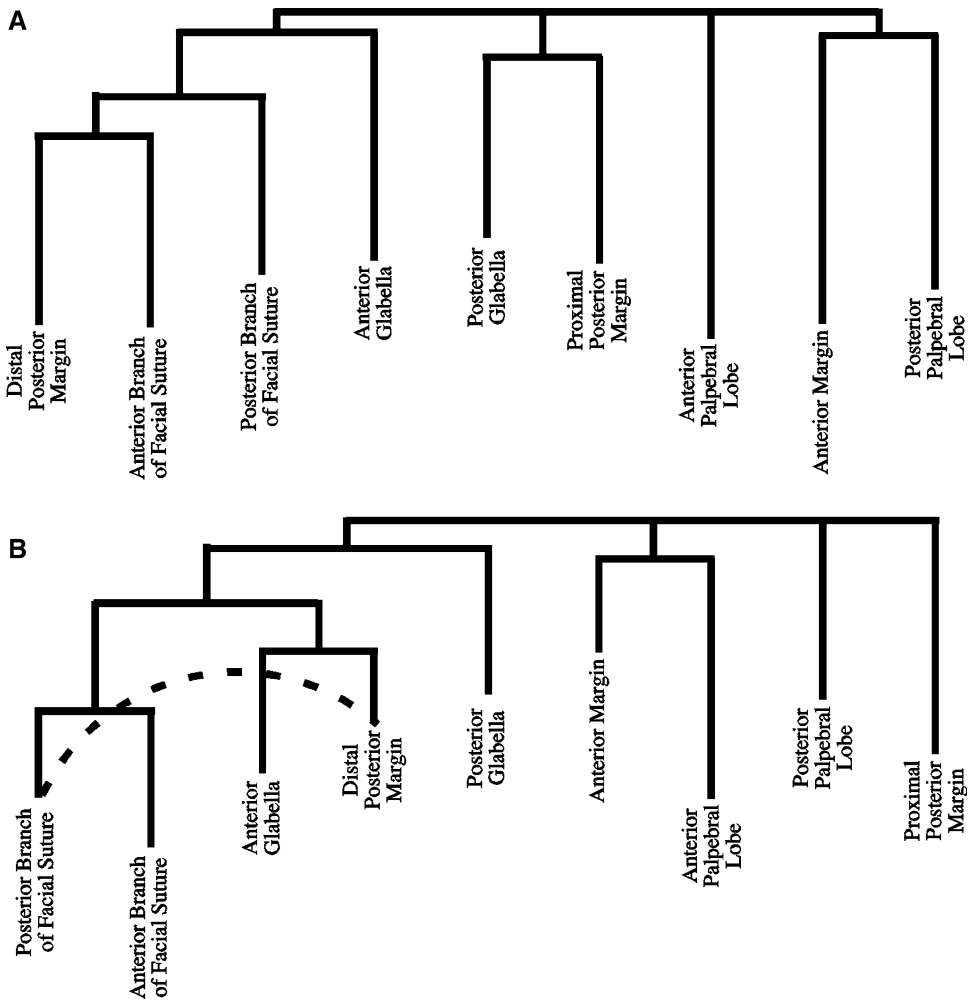

Fig. 4 Reticulograms depicting relationships among partitions for the **a** Individuals and **b** FA components of variation in *Eokochaspis nodosa*. Partitions shown in Fig. 2b

congruent with that seen in the corresponding reticulogram. An edge connects the posterior glabella to the proximal posterior margin partition, and edges also connect the distal posterior margin to each branch of the facial suture, although these two facial suture partitions are not connected to each other. Edges connect the anterior glabella to both the posterior glabella and posterior branch of the facial suture, although these last two partitions are not connected to each other. Also consistent with the results of the reticulate network analysis, the anterior palpebral lobe is not connected to any other partition. The graphical model for the FA component of *E. nodosa* (Fig. 5d) also reveals a pattern largely congruent with that seen in the corresponding reticulogram. The two branches of the facial suture are connected, as is the distal posterior margin partition to the posterior branch of the facial suture and to both anterior and posterior glabella partitions (that are not connected to each other). Consistent with the reticulogram, the anterior margin is connected to the anterior palpebral lobe; however, edges also connect the anterior margin to the posterior glabella and the posterior palpebral lobe and these relationships are not evident in the reticulogram. A weak edge connects the posterior glabella to the proximal posterior margin. The anterior margin partition is also connected to both palpebral lobe partitions, although those are not connected to each other and the edge between the anterior margin and posterior palpebral lobe is weak.

Assessing the Contribution of Direct Interactions to Phenotypic Integration

The matrix correlation between the correlation matrices of the Individuals and FA components for *C. walcotti* is weak ($R_M = 0.211$); the matrices are no more similar than expected by chance ($P = 0.12$) and, not surprisingly, the null hypothesis that the matrices are identical is rejected (Table 6). This indicates that direct interactions did not significantly influence the structure of phenotypic integration in this species. In the case of *E. nodosa*, the

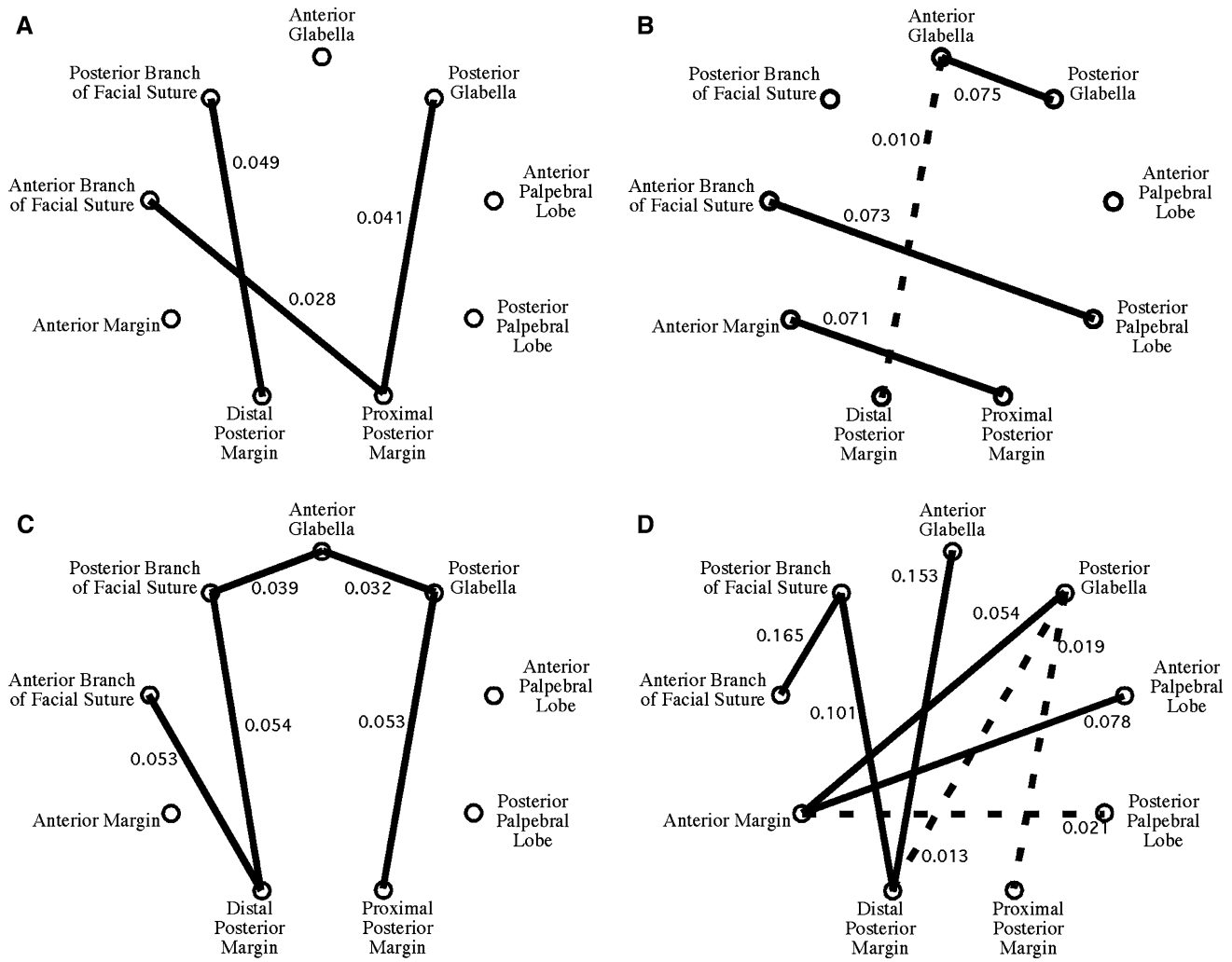

Fig. 5 Graphical models depicting empirical associations between partitions based on analysis of **a** Individuals and **b** FA components of variation in *Crassifimbra walcotti*, and **c** Individuals and **d** FA components of variation in *Eokochaspis nodosa*. *Dotted lines* indicate relatively weak edges, as indicated by edge strengths adjacent to links. Partitions shown in Fig. 2b. Model statistics: **a** deviance = 21.946; $df = 33$; $P = 0.929$; AIC = 924.729; **b** deviance = 21.486; $df = 32$; $P = 0.920$; AIC = 914.358; **c** deviance = 15.636; $df = 31$; $P = 0.990$; AIC = 911.491; **d** deviance = 13.596; $df = 28$; $P = 0.990$; AIC = 860.794

Table 6 Matrix correlation between correlation matrices derived from the Individuals and FA components of variation for *C. walcotti*, *E. nodosa*, and *C.*? *metalaspis*

Species	Observed matrix correlation	Repeatability		Probability of matrices being identical	
		Individuals component	FA component	Individuals component	FA component
C. walcotti	0.211	0.564	0.600	0.253	0.183
E. nodosa	0.386	0.590	0.765	0.563	0.074
C.? *metalaspis*	0.448	0.849	0.822	0.005	0.030

Repeatability of each correlation matrix is assessed by 2,000 bootstraps. Probability of the matrices being identical is assessed by 1,000 bootstraps, using method described in text

moderately weak but statistically significant matrix correlation between the Individuals and FA components ($R_M = 0.386$, $P = 0.02$) indicates that direct interactions did contribute to the structure of phenotypic integration. However, the two matrices are statistically significantly more different than expected by chance (Table 6), as was

Table 7 Pairwise interspecific comparisons of structures of correlation matrices (derived from the Individuals or FA components of variation) using matrix correlation

Species 1	Species 2	Component	Observed matrix correlation	Repeatability		Probability of matrices being identical	
				Species 1	Species 2	Species 1	Species 2
C. walcotti	*E. nodosa*	Individuals	0.148	0.559	0.592	0.149	0.118
C.? metalaspis	*E. nodosa*	Individuals	0.271	0.848	0.592	0	0.284
C.? metalaspis	*C. walcotti*	Individuals	0.334	0.849	0.559	0	0.535
C. walcotti	*E. nodosa*	FA	0.072	0.597	0.761	0.045	0
C.? metalaspis	*E. nodosa*	FA	0.665	0.826	0.765	0.417	0.72
C.? metalaspis	*C. walcotti*	FA	0.144	0.824	0.595	0	0.098

Repeatability of each correlation matrix is assessed by 2,000 bootstraps. Probability of the matrices being identical is assessed by 1,000 bootstraps, using method described in text

also found in the case of *C.? metalaspis* (Webster and Zelditch 2011; summarized in Table 6).

Comparing the Structure of Integration Among Species

Individuals Component

The correlation matrices of the Individuals component of *C. walcotti* and *E. nodosa* are no more similar than expected by chance ($R_M = 0.148$, $P = 0.191$), and those of *E. nodosa* and *C.? metalaspis* are only very weakly similar ($R_M = 0.271$, $P = 0.072$). The correlation matrices of the Individuals component of *C. walcotti* and *C.? metalaspis* exhibit the strongest (albeit still weak) association and are more similar than expected by chance ($R_M = 0.334$, $P = 0.031$). Given these weak correlations, it is not surprising that the correlation matrices of the Individuals components of these three species differ by more than expected by chance (Table 7). Based on description and exploratory analyses of the correlation matrices (Tables 3, 4; Figs. 3, 4, 5; see Webster and Zelditch 2011 for equivalents for *C.? metalaspis*), what appears to be common to all three species is the integration between two pairs of adjacent partitions: (1) the posterior glabella and proximal posterior margin, and (2) the distal posterior margin and posterior branch of the facial suture.

FA Component of Variation

The correlation matrices of the FA component of *C. walcotti* and *E. nodosa* are no more similar than expected by chance ($R_M = 0.073$; $P = 0.345$), and so are those of *C. walcotti* and *C.? metalaspis* ($R_M = 0.144$; $P = 0.235$). However, the correlation matrices of *E. nodosa* and *C.? metalaspis* are statistically significantly similar, and quite strongly associated ($R_M = 0.665$; $P = 0.001$). Despite that relatively high degree of similarity between two of the species, *E. nodosa* and *C.? metalaspis*, all three differ in the structure of the FA component by more than expected by chance (Table 7). Based on description and exploratory analyses of the correlation matrices (Tables 3, 4; Figs. 3, 4, 5; see Webster and Zelditch 2011 for equivalents for *C.? metalaspis*), what appears to be common to all three species is the integration between two pairs of partitions: (1) the anterior glabella and distal posterior margin, and (2) the anterior margin and proximal posterior margin (although support for the latter is rather weak in *E. nodosa*). In contrast to the pattern seen in the Individuals component, the pairs of integrated partitions are not spatially adjacent. No associations other than these are shared by *C. walcotti* and *E. nodosa*. In both *Crassifimbra* species, one other feature is similar: the anterior glabella is also integrated with the posterior glabella. As might be expected from the relatively high correlation between their correlation matrices, *E. nodosa* and *C.? metalaspis* have other features in common. One is a broader cluster that contains not only the anterior glabella and distal posterior margin but also the anterior and posterior branches of the facial suture, and another is a broader cluster that contains not only the anterior margin and proximal posterior margin but also the anterior and posterior portions of the palpebral lobes.

Discussion

The three species analyzed herein were extant during the dramatic Cambrian diversification of ptychoparioid trilobites. For that reason, we expected to find that the structure of phenotypic integration would have been either unusually labile, or that direct interactions would have been relatively inconsequential in their impact on phenotypic integration. Those expectations were grounded in the premise that either the lability of integration or inconsequential direct interactions would have imposed only weak constraints on diversification at the base of the radiation. We also anticipated that functional integration would have had only a

weak impact on phenotypic integration because long-term stabilizing selection should have conserved function-dependent integration (provided that function itself was conserved). As anticipated, we find that phenotypic integration diverged to a striking extent between these closely related species, as evident from the very low correlations between correlation matrices, ranging from just 0.148 to 0.334. Even the higher correlation, found between the two congeneric species, is lower than that found in a comparison of mandibular integration in rodents from two different suborders, the sole study that used comparable methods to examine the impact of direct interactions on phenotypic integration (Zelditch et al. 2009). Also as anticipated, direct interactions made only a modest contribution to the structure of phenotypic integration: the correlation between the matrices of these two components ranges from just 0.211 to 0.448. Even the higher of these is lower than that found in the comparison between fox squirrel and deer mouse, which found a moderate value of 0.554 (Zelditch et al. 2009). Additionally, as expected, we find that functional integration (as encoded by our functional model) does not predict the structure of phenotypic integration, consistent with conclusions drawn in our prior study of *C.*? *metalaspis* (Webster and Zelditch 2011). Such a mismatch between functional and phenotypic integration is not unprecedented: a similar mismatch was recently found in a study of cricket wings (Klingenberg et al. 2010) and other studies have found that function is either a poor predictor of integration or that developmental theory is a better one (Lawler 2008; Armbruster et al. 1999; Herrera et al. 2002). In contrast to these largely anticipated results, a highly unexpected one is the strikingly different pattern of evolutionary change in the structure of phenotypic integration and direct interactions. Rather than the two congeneric species being most similar, but only weakly so, as they are in the structure of phenotypic integration, the interspecific correlations for integration due to direct interactions range from a very low value of 0.072 to a high of 0.665, with *E. nodosa* and *C.*? *metalaspis* being the most similar. Evidently, the strong similarity between *E. nodosa* and *C.*? *metalaspis* in the structure of direct interactions did not constrain the divergence of phenotypic integration, perhaps because direct interactions made only a modest contribution to phenotypic integration.

A greater similarity between species, and also between components of integration, is found when comparisons are based on the covariances of landmarks rather than correlations between shapes. That greater similarity would be expected when integration is due, in part, to the relative sizes of parts and their positioning within the whole, neither of which contributes to the integration between shapes of the parts (Klingenberg 2009). Comparisons of phenotypic integration between these trilobite species based covariance matrices of landmarks show a moderate to high degree of similarity in their structure of phenotypic integration in that all correlations exceed 0.63. These values are comparable to those found between covariance matrices of murid rodent cranial landmarks (Jamniczky and Hallgrímsson 2009), although the timescales of divergence are obviously not comparable between the studies. Direct interactions made only a modest contribution to phenotypic integration in these trilobites when assessed by the covariances among landmarks, just as they did in analyses based on correlations between parts: these correlations for landmark covariance matrices yield values ranging from just 0.22 to 0.38. These are not the lowest values reported to date—far lower values of this measure or of others used to compare the covariance matrices are given for studies of mammalian crania (Debat et al. 2000; Willmore et al. 2005), and a comparable value is found for the house mouse mandible in one study (Klingenberg et al. 2003). However, a greater impact of direct interactions on phenotypic integration is reported in other studies of mammalian mandibles (Badyaev and Foresman 2000; Young and Badyaev 2006; Zelditch et al. 2008, 2009) and a far greater impact of direct interactions is typically found in studies of insect wings (Klingenberg and McIntyre 1998; Klingenberg and Zaklan 2000; Klingenberg et al. 2001, 2010; Breuker et al. 2007; although see Santos et al. 2005; Debat et al. 2006 for exceptions). The covariance structure of direct interactions indicates moderate to high similarity between species, with correlations ranging from 0.53 to 0.85, with the greatest similarity again found between *E. nodosa* and *C.*? *metalaspis*. That higher value is high relative to the one found between direct interactions of wolf crania compared to domestic dogs (Drake and Klingenberg 2010), but the range of values found in the present study suggests that direct interactions need not be highly conserved. The findings from the analyses of landmark covariances thus largely concur with those based correlations between shapes: (1) phenotypic integration was hardly conserved over the approximately 1 million years during which these species diverged; (2) direct interactions made only a modest contribution to phenotypic integration; (3) direct interactions can be, but need not be, highly conserved; and, more surprisingly, (4) the conservation of direct interactions had little impact on the evolutionary dynamics of phenotypic integration in these early ptychoparioids. Species that were most similar in the structure of integration due to direct interactions were not the ones that were most similar in the structure of phenotypic integration.

Three caveats should be noted. First, our conclusions regarding the structure of direct interactions in *C. walcotti* must be treated with caution because of the relatively weak signal of the FA component of variation in that species.

Second, and perhaps more importantly, our analyses are based on the a priori division of the cranidium into the nine partitions, which are taken out of context of the whole. This a priori partitioning places a premium on the recognition and biological significance of partition boundaries, and taking the shapes out of context of the whole ignores integration due to position and relative size of the partitions. Although boundaries between these partitions can be defended on biological grounds, future studies could employ methods that do not depend on such a priori partitioning (Márquez 2008; Klingenberg 2009). Third, functional integration may have played a larger role than was detected herein, because our model of functional integration is simple and could be refined. For example, one refinement would be to permit integration between some functional modules (e.g., those involving the visual field and ecdysial mechanics, because the distal margin of the palpebral lobes is also defined by an ecdysial suture). Such refinements may show better fit to the observed data. Nevertheless, our conclusions strongly suggest that cranidial integration was primarily governed by factors other than function. Alternative models based on other factors should therefore be explored. Cranidial form must have been jointly determined by the various morphogenetic processes that shaped the underlying epidermal tissue, and by the factors regulating the spatial patterning of calcification and thus the location of ecdysial sutures.

The inability to directly study and experimentally manipulate processes involved in trilobite cranidial development places obvious limits on our ability to formulate a priori developmental models. Nevertheless, we are optimistic that such models can be reasonably developed in the not too distant future. For example, Hox genes play a critical role in regulating development of segment-specific structures and organs, and models of Hox gene expression domains have been proposed for the axial region of trilobites (Sundberg 2000; Hughes 2003a, b). A hypothesis for integration based on Hox expression domains cannot be applied to the whole cranidium because we presently lack complete knowledge of the lateral course of segments away from the glabella. However, ongoing study of the ontogeny of olenelloid trilobites, that retain some traces of segmentation in the abaxial portion of the cephalon during early ontogeny, may help resolve this issue (e.g., Webster 2007). Similarly, understanding of the controls over cuticle calcification in arthropods is improving (e.g., Priester et al. 2005; Shafer et al. 2006; Inoue et al. 2008). If models for regulation of ecdysial suture location and form are ultimately developed for modern arthropods, the possibility of extending those models to trilobites should be explored. The exploratory analyses presented herein reveal that many instances of phenotypic integration among cranidial regions (including both that are common to all three species) involve neighboring partitions. These aspects of integration may have arisen from localized morphogenetic controls. Analogous "neighborhood effects" in integration have been noted in several studies of extant taxa (Chernoff and Magwene 1999; Klingenberg and Zaklan 2000; Klingenberg et al. 2001, and references therein; Zelditch et al. 2009). However, many other instances of integration detected here (including both instances of direct interactions that are common to all three species) do not involve spatially adjacent partitions. Of course, given the complexity of the sclerite, trilobite cranidial integration may have been governed by more than one underlying factor.

We anticipated that these trilobites would be relatively unconstrained in their potential for morphological diversification because they are at the base of a major diversification. The obvious question is whether these early trilobites are any less constrained than later (post-radiation) ones. The hypothesis that integration influences evolvability over short evolutionary timescales is well supported by theory and empirical data (e.g., Simpson 1944; Burger 1986; Wagner 1988; Wagner and Altenberg 1996; Schluter 1996; Marroig and Cheverud 2005; Renaud et al. 2006; Sniegowski and Murphy 2006; Hunt 2007). The extent to which the structure of integration is conserved through deep time can be inferred from comparison over a broad sampling of extant taxa (e.g., Goswami 2006a, b, 2007), but the fossil record offers a more direct documentation of phylogenetic conservatism and this has yet to be exploited. Our analysis represents a step in this direction, but it bears only on the expectation that intrinsic constraints are both weak and labile at the base of a radiation. We cannot yet say whether intrinsic constraints in these three ptychoparioids were weak for trilobites in general, because these are the only trilobites yet studied. Another outstanding question is whether the structures of phenotypic and functional integration become increasingly similar through time, making it more likely that stabilizing selection would then conserve the structure of phenotypic integration. We would not expect that particular selective constraint on integration to have been in place during the initial radiation of ptychoparioids because, to the extent that our simple model of functional integration is realistic, we find no such match in the species studied herein. Fortunately, the exquisite preservational mode represented by these early ptychoparioids was not unique to this time interval, and future comparative analyses can reveal whether intrinsic constraints are either more severe or more conservative in younger trilobites.

Acknowledgments H. D. Sheets fixed a bug in the SemiLand software at short notice and provided helpful technical comments regarding size-standardization. Some of the material analyzed herein was collected by A. R. (Pete) Palmer. Assistance to MW in the field was generously provided by N. C. Hughes, R. R. Gaines, L.

McCollum, and M. McCollum. Code for performing the bootstrapping procedure was devised by A. Haber as part of her Ph.D. thesis (University of Chicago); her generosity in providing the code is greatly appreciated. We thank two anonymous reviewers for their comments.

Appendix

Phylogenetic Relatedness of the Species

Crassifimbra walcotti is very closely related to *Crassifimbra*? *metalaspis* (see comments in Webster 2011), and their coeval stratigraphic occurrence in the uppermost Dyeran suggests very recent common ancestry. (The provisional assignment of the latter species to *Crassifimbra* [and hence the use of the "?" in the name] reflects the needs for a full systematic revision of that genus and other poorly diagnosed antagmine ptychoparioid genera, as discussed by Webster 2011.) *Eokochaspis nodosa* occurs in slightly younger sediments (basal bed of the Delamaran). Phylogenetic analysis places *E. nodosa* as a member of a kochaspid clade separated from the two species of *Crassifimbra* by nine internal nodes, although branch lengths were very short (Sundberg 2004; Webster 2011; unpublished data). A new species representing the oldest kochaspid (to be described elsewhere) occurs at very low abundance in collections with *C.*? *metalaspis*. Phylogenetic analyses and stratigraphic data therefore suggest that *E. nodosa* shared a last common ancestor with *Crassifimbra* in the late Dyeran.

Assigning absolute time to these phylogenetic branches is necessarily speculative because the strata sampled here are inappropriate for radiometric dating and there are very few radiometric dates compiled worldwide for strata of this age interval. However, the base of the Delamaran is approximately 510 million years old, and beds from New Brunswick dated as 511 $\pm$1 million years old approximately correlate to the upper Dyeran (Landing et al. 1998; Shergold and Cooper in Gradstein et al. 2004). Given that the oldest known occurrences of *C. walcotti*, *C.*? *metalaspis*, and the kochaspid clade are stratigraphically coeval in the uppermost Dyeran, we infer that (1) there is on the order of just a few tens of thousands to hundreds of thousands of years between the sampled occurrence of the two *Crassifimbra* species and their last common ancestor; (2) branch length between the last common ancestor of the two *Crassifimbra* species and the last common ancestor of [*Crassifimbra* + the kochaspid clade] is also on the order of just a few tens of thousands to hundreds of thousands of years; and (3) there is $\approx$1 million years separating *E. nodosa* from its last common ancestor with *Crassifimbra*. Such estimates are consistent with available phylogenetic and stratigraphic data (Sundberg 2004; Webster 2011; unpublished data), and apply minimal insult to the fidelity of the trilobite fossil record.

References

Akaike, H. (1974). A new look at the statistical model identification. *IEEE Transactions on Automatic Control, 19*(6), 716–723.

Allen, C. E. (2008). The "eyespot" module and eyespots and modules: Development, evolution, and integration of a complex phenotype. *Journal of Experimental Zoology, Part B: Molecular and Developmental Evolution, 310B*(2), 179–190.

Armbruster, W. S., Di Stilio, V. S., Tuxill, J. D., Flores, T. C., & Runk, J. L. V. (1999). Covariance and decoupling of floral and vegetative traits in nine neotropical plants: A re-evaluation in Berg's correlation pleiades concept. *American Journal of Botany, 86*(1), 39–55.

Auffray, J.-C., Alibert, P., Renaud, S., Orth, A., & Bonhomme, F. (1996). Fluctuating asymmetry in *Mus musculus* subspecific hybridization: Traditional and procrustes comparative approaches. In L. F. Marcus, M. Corti, A. Loy, G. J. P. Naylor, & D. E. Slice (Eds.), *Advances in morphometrics. Nato ASI series, series A: Life science* (pp. 275–284). New York: Plenum Press.

Badyaev, A. V., & Foresman, K. R. (2000). Extreme environmental change and evolution: Stress-induced morphological variation is strongly concordant with patterns of evolutionary divergence in shrew mandibles. *Proceedings of the Royal Society on London, Series B Biological Sciences, 267*(1441), 371–377.

Badyaev, A. V., & Foresman, K. R. (2004). Evolution of morphological integration. I. Functional units channel stress-induced variation in shrew mandibles. *American Naturalist, 163*(6), 868–879.

Breuker, C. J., Gibbs, M., Van Dyck, H., Brakefield, P. M., Klingenberg, C. P., & Van Dongen, S. (2007). Integration of wings and their eyespots in the speckled wood butterfly *Pararge aegeria*. *Journal of Experimental Zoology, Part B: Molecular and Developmental Evolution, 308B*(4), 454–463.

Breuker, C. J., Patterson, J. S., & Klingenberg, C. P. (2006). A single basis for developmental buffering of *Drosophila* wing shape. *PLoS One, 1*, e7.

Burger, R. (1986). Constraints for the evolution of functionally coupled characters: A nonlinear analysis of a phenotypic model. *Evolution, 40*, 182–193.

Chernoff, B., & Magwene, P. M. (1999). Afterword. Morphological integration: Forty years later. In E. C. Olson & R. L. Miller (Eds.), *Morphological integration* (pp. 319–353). Chicago: University of Chicago Press.

Cheverud, J. M. (1982). Phenotypic, genetic, and environmental morphological integration in the cranium. *Evolution, 36*(3), 499–516.

Cheverud, J. M. (1984). Quantitative genetics and developmental constraints on evolution by selection. *Journal of Theoretical Biology, 110*, 155–171.

Cheverud, J. M., & Marroig, G. (2007). Comparing covariance matrices: Random skewers method compared to the common principal components model. *Genetics and Molecular Biology, 30*, 461–469.

Cowley, D. E., & Atchley, W. R. (1990). Development and quantitative genetics of correlation structure among body parts of *Drosophila melanogaster*. *American Naturalist, 135*(2), 242–268.

Debat, V., Alibert, P., David, P., Paradis, E., & Auffray, J.-C. (2000). Independence between developmental stability and canalization in the skull of the house mouse. *Proceedings of the Royal Society of London Series B: Biological Sciences, 267*, 423–430.

Debat, V., Milton, C. C., Rutherford, S., Klingenberg, C. P., & Hoffmann, A. A. (2006). Hsp90 and the quantitative variation of wing shape in *Drosophila melanogaster*. *Evolution, 60*(12), 2529–2538.

Dietz, E. J. (1983). Permutation tests for association between two distance matrices. *Systematic Zoology, 32*(1), 21–26.

Drake, A. G., & Klingenberg, C. P. (2010). Large-scale diversification of skull shape in domestic dogs: Disparity and modularity. *American Naturalist, 175*(3), 289–301.

Edwards, D. (2008). MIM: A program for graphical modeling. Version 3.2.0.7. Hypergraph Software.

Foote, M. (1989). Perimeter-based Fourier analysis: A new morphometric method applied to the trilobite cranidium. *Journal of Paleontology, 63*(6), 880–885.

Foote, M. (1990). Nearest-neighbor analysis of trilobite morphospace. *Systematic Zoology, 39*(4), 371–382.

Foote, M. (1991). Morphologic patterns of diversification: Examples from trilobites. *Palaeontology, 34*(2), 461–485.

Foote, M. (1993a). Discordance and concordance between morphological and taxonomic diversity. *Paleobiology, 19*(2), 185–204.

Foote, M. (1993b). Contributions of individual taxa to overall morphological disparity. *Paleobiology, 19*(4), 403–419.

Fortey, R. A. (2001). Trilobite systematics: The last 75 years. *Journal of Paleontology, 75*(6), 1141–1151.

Goswami, A. (2006a). Cranial modularity shifts during mammalian evolution. *American Naturalist, 168*(2), 270–280.

Goswami, A. (2006b). Morphological integration in the carnivoran skull. *Evolution, 60*(1), 169–183.

Goswami, A. (2007). Phylogeny, diet, and cranial integration in Australodelphian marsupials. *PLOS One, 2*(10), e995.

Gradstein, F. M., Ogg, J. G., & Smith, A. G. (Eds.). (2004). *A geologic time scale 2004*. England: Cambridge University Press.

Hallgrímsson, B., Brown, J. J. Y., Ford-Hutchinson, A. F., Sheets, H. D., Zelditch, M. L., & Jirik, F. R. (2006). The brachymorph mouse and the developmental-genetic basis for canalization and morphological integration. *Evolution and Development, 8*(1), 61–73.

Hallgrímsson, B., Willmore, K., Dorval, C., & Cooper, D. M. L. (2004). Craniofacial variability and modularity in macaques and mice. *Journal of Experimental Zoology, Part B: Molecular and Developmental Evolution, 302B*, 207–225.

Herrera, C. M., Cerda, X., Garcia, M. B., Guitian, J., Medrano, M., Rey, P. J., et al. (2002). Floral integration, phenotypic covariance structure and pollinator variation in bumblebee-pollinated *Helleborus foetidus*. *Journal of Evolutionary Biology, 15*(1), 108–121.

Hughes, N. C. (2003a). Trilobite body patterning and the evolution of arthropod tagmosis. *BioEssays, 25*(4), 386–395.

Hughes, N. C. (2003b). Trilobite tagmosis and body patterning from morphological and developmental perspectives. *Integrative and Comparative Biology, 43*, 185–206.

Hunt, G. (2007). Evolutionary divergence in directions of high phenotypic variance in the ostracode genus *Poseidonamicus*. *Evolution, 61*(7), 1560–1576.

Inoue, H., Yuasa-Hashimoto, N., Suzuki, M., & Nagasawa, H. (2008). Structural determination and functional analysis of a soluble matrix protein associated with calcification of the exoskeleton of the crayfish, *Procambarus clarkii*. *Bioscience, Biotechnology, and Biochemistry, 72*(10), 2697–2707.

Jamniczky, H. A., & Hallgrímsson, B. (2009). A comparison of covariance structure in wild and laboratory muroid crania. *Evolution, 63*(6), 1540–1556.

Jernigan, R. W., Culver, D. C., & Fong, D. W. (1994). The dual role of selection and evolutionary history as reflected in genetic correlations. *Evolution, 48*(3), 587–596.

Kingsolver, J. G., & Wiernasz, D. C. (1987). Dissecting correlated characters: Adaptive aspects of phenotypic covariation in melanization pattern of *Pieris* butterflies. *Evolution, 41*(3), 491–503.

Klingenberg, C. P. (2004). Integration, modules, and development: Molecules to morphology to evolution. In M. Pigliucci & K. A. Preston (Eds.), *Phenotypic integration: Studying the ecology and evolution of complex phenotypes* (pp. 213–230). Oxford: Oxford University Press.

Klingenberg, C. P. (2005). Developmental constraints, modules, and evolvability. In B. Hallgrímsson & B. K. Hall (Eds.), *Variation: A central concept in biology* (pp. 219–247). Burlington, MA: Elsevier Academic Press.

Klingenberg, C. P. (2008). Morphological integration and developmental modularity. *Annual Review of Ecology, Evolution, and Systematics, 39*, 115–132.

Klingenberg, C. P. (2009). Morphometric integration and modularity in configurations of landmarks: Tools for evaluating a priori hypotheses. *Evolution & Development, 11*(4), 405–421.

Klingenberg, C. P., Badyaev, A. V., Sowry, S. M., & Beckwith, N. J. (2001). Inferring developmental modularity from morphological integration: Analysis of individual variation and asymmetry in bumblebee wings. *American Naturalist, 157*(1), 11–23.

Klingenberg, C. P., Barluenga, M., & Meyer, A. (2002). Shape analysis of symmetric structures: Quantifying variation among individuals and asymmetry. *Evolution, 56*(10), 1909–1920.

Klingenberg, C. P., Debat, V., & Roff, D. A. (2010). Quantitative genetics of shape in cricket wings: Developmental integration in a functional structure. *Evolution, 64*, 2935–2951.

Klingenberg, C. P., & McIntyre, G. S. (1998). Geometric morphometrics of developmental instability: Analyzing patterns of fluctuating asymmetry with procrustes methods. *Evolution, 52*(5), 1363–1375.

Klingenberg, C. P., Mebus, K., & Auffray, J.-C. (2003). Developmental integration in a complex morphological structure: How distinct are the modules in the mouse mandible? *Evolution & Development, 5*(5), 522–531.

Klingenberg, C. P., & Zaklan, S. D. (2000). Morphological integration between developmental compartments in the *Drosophila* wing. *Evolution, 54*(4), 1273–1285.

Landing, E., Bowring, S. A., Davidek, K. L., Westrop, S. R., Geyer, G., & Heldmaier, W. (1998). Duration of the early cambrian: U-Pb ages of volcanic ashes from Avalon and Gondwana. *Canadian Journal of Earth Sciences, 35*, 329–338.

Lawler, R. R. (2008). Morphological integration and natural selection in the postcranium of wild Verreaux's sifaka (*Propithecus verreauxi verreauxi*). *American Journal of Physical Anthropology, 136*, 204–213.

Leamy, L. (1984). Morphometric studies in inbred and hybrid house mice. 5. Directional and fluctuating asymmetry. *American Naturalist, 123*, 579–593.

Magwene, P. M. (2001). New tools for studying integration and modularity. *Evolution, 55*(9), 1734–1745.

Magwene, P. M. (2009). Statistical methods for studying modularity: A reply to Mitteroecker and Bookstein. *Systematic Biology, 58*(1), 146–149.

Makarenkov, V. (2000). T-REX. Version 4.0a1. Available at http://www.labunix.uqam.ca/~makarenv/trex.html.

Makarenkov, V., & Legendre, P. (2004). From a phylogenetic tree to a reticulated network. *Journal of Computational Biology, 11*(1), 195–212.

Makarenkov, V., Legendre, P., & Desdevises, Y. (2004). Modelling phylogenetic relationships using reticulated networks. *Zoologica Scripta, 33*(1), 89–96.

Mantel, N. (1967). The detection of disease clustering and a generalized regression approach. *Cancer Research, 27*(2), 209–220.

Márquez, E. (2007a). SAGE, version 1.03. Available at http://www-personal.umich.edu/~emarquez/morph/index.html.

Márquez, E. (2007b). CORIANDIS. Available at http://www-personal.umich.edu/~emarquez/morph/index.html.

Márquez, E. J. (2008). A statistical framework for testing modularity in multidimensional data. *Evolution, 62*(10), 2688–2708.

Marroig, G., & Cheverud, J. M. (2005). Size as a line of least evolutionary resistance: Diet and adaptive morphological radiation in new world monkeys. *Evolution, 59*, 1128–1142.

Mitteroecker, P., & Bookstein, F. (2007). The conceptual and statistical relationship between modularity and morphological integration. *Systematic Biology, 56*(5), 818–836.

Mitteroecker, P., & Bookstein, F. L. (2009). Examining modularity via partial correlations: A rejoinder to a comment by Paul Magwene. *Systematic Biology, 58*(3), 346–348.

Monteiro, L. R., Bonato, V., & dos Reis, S. F. (2005). Evolutionary integration and morphological diversification in complex morphological structures: Mandible shape divergence in spiny rats (Rodentia, Echimyidae). *Evolution & Development, 7*(5), 429–439.

Olson, E. C., & Miller, R. L. (1958). *Morphological integration*. Chicago: University of Chicago Press.

Palmer, A. R., & Strobeck, C. (1986). Fluctuating asymmetry—Measurement, analysis, patterns. *Annual Review of Ecology and Systematics, 17*, 391–421.

Polanski, J. M., & Franciscus, R. G. (2006). Patterns of craniofacial integration in extant *Homo*, *Pan*, and *Gorilla*. *American Journal of Physical Anthropology, 131*(1), 38–49.

Priester, C., Dillaman, R. M., & Gay, D. M. (2005). Ultrastructure, histochemistry, and mineralization patterns in the ecdysial suture of the blue crab, *Callinectes sapidus*. *Microscopy and Microanalysis, 11*, 479–499.

Renaud, S., Auffray, J.-C., & Michaux, J. (2006). Conserved phenotypic variation patterns, evolution along lines of least resistance, and departure due to selection in fossil rodents. *Evolution, 60*, 1701–1717.

Resser, C. E. (1937). Third contribution to nomenclature of Cambrian trilobites. *Smithsonian Miscellaneous Collections, 95*(22), 1–29.

Riedl, R. (1978). *Order in living organisms: A systems analysis of evolution*. New York: Wiley.

Rohlf, F. J. (2009). tpsDig. Version 2.14. Department of Ecology and Evolution, State University of New York. Available at http://life.bio.sunysb.edu.morph/.

Santos, M., Iriarte, P. F., & Cespedes, W. (2005). Genetics and geometry of canalization and developmental stability in *Drosophila subobscura*. *BMC Evolutionary Biology, 5*, 7.

Sattath, S., & Tversky, A. (1977). Additive similarity trees. *Psychometrika, 42*(3), 319–345.

Schlosser, G., & Wagner, G. P. (Eds.). (2004). *Modularity in development and evolution*. Chicago: University of Chicago Press.

Schluter, D. (1996). Adaptive radiation along genetic lines of least resistance. *Evolution, 50*(5), 1766–1774.

Shafer, T. H., McCartney, M. A., & Faircloth, L. M. (2006). Identifying exoskeleton proteins in the blue crab from an expressed sequence tag (EST) library. *Integrative and Comparative Biology, 46*(6), 978–990.

Shaw, A. B. (1957). Quantitative trilobite studies II. Measurement of the dorsal shell of non-agnostidean trilobites. *Journal of Paleontology, 31*(1), 193–207.

Sheets, H. D. (2001). Standard6beta. Department of Physics, Canisius College, Buffalo, New York. Available at http://www.canisius.edu/~sheets/morphsoft.html.

Sheets, H. D. (2009). SemiLand6. 7th Beta Version. Department of Physics, Canisius College, Buffalo, New York. Available at http://www.canisius.edu/~sheets/morphsoft.html.

Simpson, G. G. (1944). *Tempo and mode in evolution*. New York: Columbia University Press.

Sniegowski, P. D., & Murphy, H. A. (2006). Evolvability. *Current Biology, 16*(19), R831–R834.

Sundberg, F. A. (2000). Homeotic evolution in Cambrian trilobites. *Paleobiology, 26*(2), 258–270.

Sundberg, F. A. (2004). Cladistic analysis of early-middle Cambrian kochaspid trilobites (Ptychopariida). *Journal of Paleontology, 78*(5), 920–940.

Sundberg, F. A., & McCollum, L. B. (2000). Ptychopariid trilobites of the lower-middle Cambrian boundary interval, Pioche Shale, southeastern Nevada. *Journal of Paleontology, 74*(4), 604–630.

Wagner, G. P. (1988). The influence of variation and of developmental constraints on the rate of multivariate phenotypic evolution. *Journal of Evolutionary Biology, 1*, 45–66.

Wagner, G. P., & Altenberg, L. (1996). Complex adaptations and the evolution of evolvability. *Evolution, 50*(3), 967–976.

Webster, M. (2007). Ontogeny and evolution of the early Cambrian trilobite genus *Nephrolenellus* (Olenelloidea). *Journal of Paleontology, 81*(6), 1168–1193.

Webster, M. (2011). The structure of cranidial shape variation in three early ptychoparioid trilobite species from the Dyeran-Delamaran (traditional "Lower-Middle" Cambrian) boundary interval of Nevada, U.S.A. *Journal of Paleontology, 85*(2), 179–225.

Webster, M., & Zelditch, M. L. (2011). Modularity of a Cambrian ptychoparioid trilobite cranidium. *Evolution & Development, 13*(1), 96–109.

Whittington, H. B., Chatterton, B. D. E., Speyer, S. E., Fortey, R. A., Owens, R. M., Chang, W. T., et al. (1997). *Treatise on invertebrate paleontology. Part O. Arthropoda 1. Trilobita, revised. Volume 1: Introduction, order Agnostida, order Redlichiida*. Boulder, CO and Lawrence, KS: Geological Society of America and University of Kansas.

Willmore, K. E., Klingenberg, C. P., & Hallgrímsson, B. (2005). The relationship between fluctuating asymmetry and environmental variance in rhesus macaque skulls. *Evolution, 59*(4), 898–909.

Young, N. (2004). Modularity and integration in the hominoid scapula. *Journal of Experimental Zoology, Part B: Molecular and Developmental Evolution, 302B*(3), 226–240.

Young, R. L., & Badyaev, A. V. (2006). Evolutionary persistence of phenotypic integration: Influence of developmental and functional relationships on complex trait evolution. *Evolution, 60*(6), 1291–1299.

Young, N. M., & Hallgrímsson, B. (2005). Serial homology and the evolution of mammalian limb covariation structure. *Evolution, 59*(12), 2691–2704.

Zelditch, M. L., & Carmichael, A. C. (1989). Ontogenetic variation in patterns of developmental and functional integration in skulls of *Sigmodon fulviventer*. *Evolution, 43*(4), 814–824.

Zelditch, M. L., Wood, A. R., Bonett, R. M., & Swiderski, D. L. (2008). Modularity of the rodent mandible: Integrating bones, muscles, and teeth. *Evolution & Development, 10*(6), 756–768.

Zelditch, M. L., Wood, A. R., & Swiderski, D. L. (2009). Building developmental integration into functional systems: Function-induced integration of mandibular shape. *Evolutionary Biology, 36*, 71–87.